Femtosecond fluorescence upconversion spectroscopy of vapor-deposited tris(8-hydroxyquinoline) aluminum films

W. Humbs [1], H. Zhang, M. Glasbeek *

Laboratory for Physical Chemistry, University of Amsterdam, Nieuwe Achtergracht 129, 1018 WS Amsterdam, Netherlands

Abstract

Vapor-deposited Alq_3 is used as the green emitting layer in a class of organic light-emitting diodes. In this paper, the time dependence of the fluorescence from thin Alq_3 films has been studied by means of the femtosecond fluorescence upconversion technique. From the temporally resolved emission spectra, obtained after spectral reconstruction, the existence of different emissive sites in the Alq_3 film is concluded. They are identified as shallow and deep trapping sites. The average shallow trap excitation energy is located about 160 cm^{-1} below the (quasi-) exciton band, while the deep trap excitation energy is lower by approximately 2000 cm^{-1}. Above 75 K, the shallow trap excitation is thermally depleted, via the (quasi-) exciton band, to fast-trapping non-emissive sites. At liquid helium temperatures, the depletion of the highest-lying shallow traps is frozen out. At room temperature, the lifetime of the shallow traps varies from about 1 to 20 ps; the lifetime of the deep traps is about 10 ns. © 2000 Elsevier Science B.V. All rights reserved.

1. Introduction

Thin films of vapor-deposited metal chelates, such as aluminum(III) 8-hydroxyquinoline (Alq_3), have been successfully applied as emitting layers in organic light emitting diodes (OLED) [1–7]. On account of their wide-spectrum display performance, chemical stability and relatively simple device architecture, these OLEDs show advantages compared to the conventional inorganic semiconductor materials [8]. To better understand the mechanisms and the dynamics of charge injection, charge transport, and charge recombination, sev-

eral studies concerning the excited states of Alq_3 have been undertaken [9–15]. In deposited films, Alq_3 gives rise to a bright fluorescence after either electron injection or photoexcitation. The lowest excited state is localized at one of the quinolinolate ligands (for molecular structure, see insert in Fig. 1). At this ligand site, the electronic charge has been partially transferred from the phenoxide to the pyridyl ring (intraligand charge transfer) [2,14–16].

In liquid solution, photoinduced fluorescence of Alq_3 has also been observed [1,9]. The decay of the fluorescence is exponential with a typical lifetime of 10 ns at room temperature. In a previous paper [17], we reported picosecond components in the fluorescence decay. It was shown that a fast dynamic Stokes shift occurs after pulsed laser excitation of Alq_3 and Gaq_3 dissolved in liquid solution. The dynamic Stokes shift was attributed to solvation dynamics. It was verified that

* Corresponding author. Tel.: +31-20-5256996; fax: +31-20-5256994.

  E-mail address: glasbeek@fys.chem.uva.nl (M. Glasbeek).

  [1] Present address: Samsung SDI, European Research Center, 12459 Berlin, Germany.
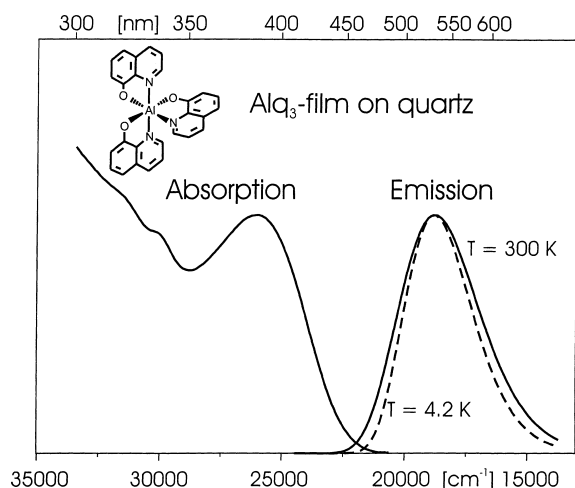
Fig. 1. Absorption and emission spectra of a 150 nm thin Alq_3 film on a quartz substrate.

the fast dynamic Stokes shift is absent for the Alq_3-complex doped into a crystalline $Al(acac)_3$ matrix.

In this paper, we study the excited state short-time dynamics of 150 nm thin Alq_3 layers, deposited on quartz substrates. (Sub)picosecond studies of Alq_3 thin films (as used in OLED devices) have so far not been reported. It will be shown that the photoemission of Alq_3 films at room temperature contains short-living ($\sim$1 to 20 ps) components originating from shallow traps.

2. Experimental

Alq_3 was purchased from Aldrich and used without further purification. Thin films were deposited on quartz slides. The substrates were cleaned as described in Ref. [4], followed by high-voltage discharging in the reaction chamber. The samples were prepared by sequential, high-vacuum ($<2 \times 10^{-6}$ Torr) vapor deposition of Alq_3 on the quartz substrate by thermal evaporation from a tungsten boat at a deposition rate of $\approx$5 Å/s. Typically, the thickness of the Alq_3 layer was 150 nm. Freshly prepared films were stored under nitrogen atmosphere in a desiccator. From measurements of the absorption and emission signal intensities before and after each series of transient measurements, it was verified that no spectral de-

gradation had occurred during the measurements. Furthermore, freshly prepared samples and older samples gave the same results.

The Alq_3 samples were placed on a sample holder and introduced into a nitrogen flow cryostat for measurements in the temperature range from 77 to 300 K. For measurements at 4.2 K, a helium bath cryostat was used.

Steady-state absorption spectra were recorded by means of a conventional spectrophotometer (Shimadzu, UV-240). The steady-state fluorescence spectra were measured using the emission spectrometer described before [18]. The emission spectra were corrected for the wavelength-dependent sensitivity of the detection system.

Femtosecond and picosecond fluorescence transients were measured by means of two experimental setups, the femtosecond and picosecond fluorescence spectrometers, respectively. Femtosecond laser excitation was accomplished using a cw $Nd:YVO_4$ laser (Spectra Physics, Millennia X) that pumped a Ti:sapphire laser (Spectra Physics, Tsunami) operating at 800 nm and delivering 60 fs pulses at a repetition rate of 82 MHz. The fs laser pulses were first amplified in a regenerative amplifier laser system (Quantronix) to about 400 mW at 1 kHz, and then split into two beams. The first of these beams was led into an OPA laser system (Light Conversion Ltd.). The pulses from the OPA laser were used for photoexcitation of the sample. In the femtosecond upconversion experiments, the excitation wavelength was tunable from 300 to 390 nm.

The ensuing transient fluorescence was time-resolved detected applying the fluorescence upconversion detection technique [19,20]. To accomplish this, the split-off second (gating) beam from the regenerative amplifier (800 nm), was led through a delay line and focused together with the pump-pulse induced fluorescence onto a BBO crystal (type I phase matching condition). The upconversion signal (at the sum frequency of the fluorescence and the gating beam) was filtered out by an UG 11 filter, and then focused on the entrance slit of a Zeiss M 20 monochromator and photodetected using a photomultiplier (EMI, 9863 QB/350) connected to a lock-in amplifier system (Stanford Research Systems, SR 830). From the

measured cross-correlation function of the excitation and gating pulses, the instrumental response time was determined to be approximately 150 fs (FWHM).

Fluorescence transient measurements with picosecond time resolution were conducted using time-correlated single-photon-counting detection [18]. Briefly, a mode-locked Ar^+ ion laser (Coherent, Innova 200-15) synchronously pumped a cavity-dumped dye laser (Coherent, 702-3, DCM-Spezial (Radiant Dyes Chemie) as a dye). The dye laser generated laser pulses of about 7 ps (FWHM) and 25 nJ at 3.7 MHz. These pulses were frequency doubled in a 6 mm BBO crystal and used to photoexcite the sample. The instrumental response was about 16 ps (FWHM).

3. Results

Steady-state absorption and emission spectra at different temperatures of vapor-deposited 150 nm thin Alq_3 films on a quartz substrate are shown in Fig. 1. The maximum of the lowest intense absorption band lies at $26\,000$ cm^{-1} ($T = 300$ K). The emission band maximum is centered at $18\,850$ cm^{-1} ($T = 4.2$ and 300 K). With decreasing temperature, the emission bandwidth is reduced.

A few typical room temperature fluorescence upconversion transients of Alq_3 film at different detection wavelengths (in the range 455–608 nm) for a fixed excitation ($\lambda_{exc} = 350$ nm) are shown in Fig. 2. The fluorescence decay transients were fitted to a triexponential function, convoluted with the system response function. The slowest of the three time constants in the multi-exponential function (10.0 ns) was kept fixed in the fitting procedure. This component is considered to be characteristic of the lifetime of the fluorescent state. The tails of the fitted decay curves matched the fitted curves of the transients obtained with the time-correlated single-photon counting picosecond setup. Thus, the fluorescence transients were measured in time windows spanning from 60 ps to 50 ns. The time components (τ_i) and pre-exponential factors (a_i), as obtained for a series of detection wavelengths, are listed in Table 1. Clearly, the decay behavior of the emission is characterized
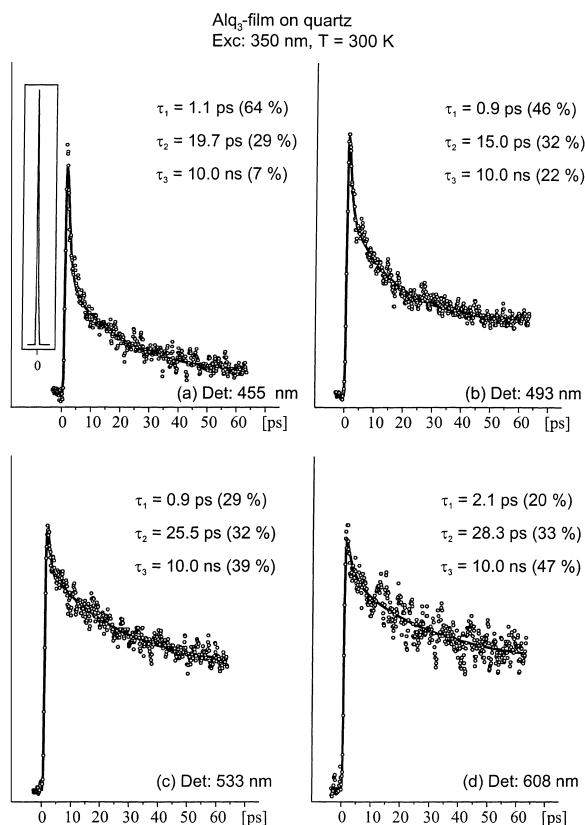
Fig. 2. Representative fluorescence transients of a 150 nm thin Alq_3 film on a quartz substrate for different detection wavelengths, excited at 350 nm, $T = 300$ K. Drawn curves represent best fits as described in the text. Time constants and pre-exponential factors are given in Table 1. The system response function is included in (a).

by two fast components and one slow decay component. The pre-exponential factors change with the detection wavelength. When detection is at the blue side of the emission spectrum ($\lambda_{det} = 455$ nm), a short-lived component, with $\tau_1 = 1.1$ ps (a_1: 64%), is dominant, while detection at the red side of the emission ($\lambda_{det} = 608$ nm) yields a dominant long-lived component with $\tau_3 = 10$ ns (a_3: 47%).

Following the spectral reconstruction method [21], time-resolved emission spectra were obtained. The squares in Fig. 3 represent the intensities $I(\lambda,t)$ of the total emission for various delay times following the excitation pulse,

Table 1

Time components (τ_i) and pre-exponential factors (a_i) for different detection wavelengths obtained from the fit of fluorescence decays of Alq$_3$ films on a quartz substrate, measured by upconversion technique in a time window of 60 ps at different detection wavelengths (system response time: 150 fs, $T = 300$ K, $\lambda_{exc} = 350$ nm)

Detection wavelength (nm)	τ_1 (ps) (a_1)	τ_2 (ps) (a_2)	τ_3 (ns) (a_3)
455	1.1 (64%)	19.7 (29%)	10.0 (7%)
468	1.0 (60%)	17.2 (31%)	10.0 (9%)
480	1.3 (55%)	22.1 (32%)	10.0 (13%)
493	0.9 (46%)	15.0 (32%)	10.0 (22%)
505	1.3 (44%)	21.0 (38%)	10.0 (18%)
520	1.5 (29%)	20.6 (39%)	10.0 (32%)
533	0.9 (29%)	25.5 (32%)	10.0 (39%)
548	1.7 (30%)	31.6 (32%)	10.0 (38%)
575	2.2 (25%)	36.0 (31%)	10.0 (44%)
590	2.0 (23%)	21.4 (30%)	10.0 (47%)
608	2.1 (20%)	28.3 (33%)	10.0 (47%)
623	2.2 (22%)	57.3 (39%)	10.0 (39%)

$$I(\lambda, t) = a_1(\lambda) \exp\left(-\frac{t}{\tau_1}\right) + a_2(\lambda) \exp\left(-\frac{t}{\tau_2}\right)$$
$$+ a_3(\lambda) \exp\left(-\frac{t}{\tau_3}\right), \qquad (1)$$

where a_i represent the pre-exponential factors and τ_i represent the decay times obtained after fitting the transients to a triexponential function. For illustrative purposes, we have included in Fig. 3 the contribution of each single exponential function of Eq. (1). The curves in the figure show the best fit of the data points (not shown for the individual components) to a log-normal line shape function [21]. Fitting with functional forms other than the triexponential decay function (e.g., biexponential decay or stretched exponential decay functions) led to results of less quality. Multi-exponential fittings with four exponential (or more) terms did not give significantly improved fittings. Thus, in the remainder of the paper, the fluorescence kinetics of the Alq$_3$ films is treated in terms of the three-exponential decay function.

The Alq$_3$ fluorescence transients were also measured as a function of the excitation wavelength keeping the detection wavelength fixed (480 nm) (Fig. 4). Note that at this detection position, emission bands I–III overlap. The respec-
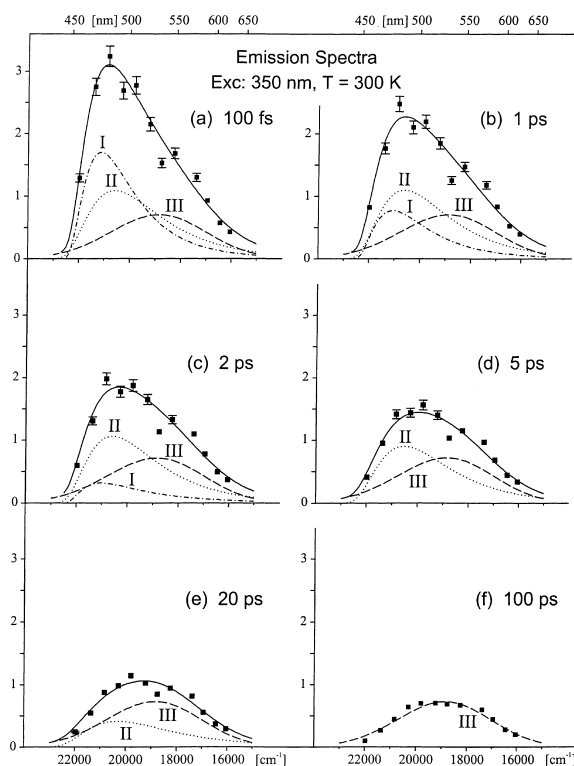
Fig. 3. Reconstructed time-resolved emission spectra of a 150 nm thin Alq$_3$ film on a quartz substrate, in the time range from 100 fs to 100 ps, excited at 350 nm, $T = 300$ K. The delay times following the excitation pulse are indicated in the panels. The squares represent the data points obtained after spectral reconstruction for the total emission intensity $I(\lambda, t) = a_1(\lambda) \exp(-t/\tau_1) + a_2(\lambda) \exp(-t/\tau_2) + a_3(\lambda) \exp(-t/\tau_3)$. The dash-dotted curve (band I) represents a log-normal fit of the reconstructed emission spectrum for the single exponential decay with τ_1, the dotted curve (band II) represents a log-normal fit of the reconstructed emission spectrum for a single exponential decay with τ_2, the dashed curve (band III) represents a log-normal fit of the reconstructed emission spectrum for a single exponential decay with τ_3. The solid curve is the sum of the individual log-normal functions.

tive time components and pre-exponential factors resulting from a triexponential fit are summarized in Table 2. The fitting procedure is the same as discussed above in Section 3. The table shows that the characteristic times, τ_1 to τ_3, remain the same within the experimental error, but the ratio of the pre-exponential factors is wavelength dependent. Following the spectral reconstruction technique, the excitation spectra detected after different delay
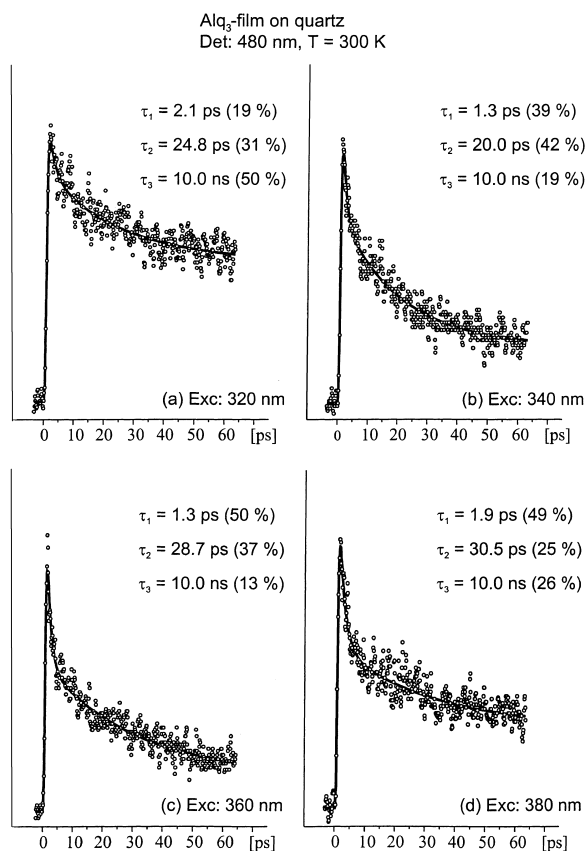
Fig. 4. Representative fluorescence transients of a 150 nm thin Alq$_3$ film on a quartz substrate for different excitation wavelengths, detection at 480 nm, $T = 300$ K. Drawn curves represent best fits as described in the text. Respective time constants and pre-exponential factors are also given in Table 2.

Table 2

Time components (τ_i) and pre-exponential factors (a_i) for different excitation wavelengths obtained from the fit of fluorescence decays of Alq$_3$ films on a quartz substrate measured by upconversion technique in a time window of 60 ps at different excitation wavelengths (system response time: 150 fs, $T = 300$ K, $\lambda_{det} = 480$ nm)

Excitation wavelength (nm)	τ_1 (ps) (a_1)	τ_2 (ps) (a_2)	τ_3 (ns) (a_3)
320	2.1 (19%)	24.8 (31%)	10.0 (50%)
330	2.3 (24%)	33.5 (44%)	10.0 (32%)
340	1.3 (39%)	19.9 (42%)	10.0 (19%)
350	1.3 (55%)	22.1 (32%)	10.0 (13%)
360	1.3 (50%)	28.7 (37%)	10.0 (13%)
370	1.3 (40%)	23.0 (37%)	10.0 (23%)
380	1.9 (49%)	30.5 (25%)	10.0 (26%)

times could be calculated. The squares in Fig. 5 represent the total intensity of the reconstructed excitation spectra. Also, the contributions of bands I–III to the total intensity of the excitation spectra can be calculated. The resulting point-to-point spectra are also included in Fig. 5.

The fluorescence transients of the Alq$_3$ films were also measured as a function of temperature.
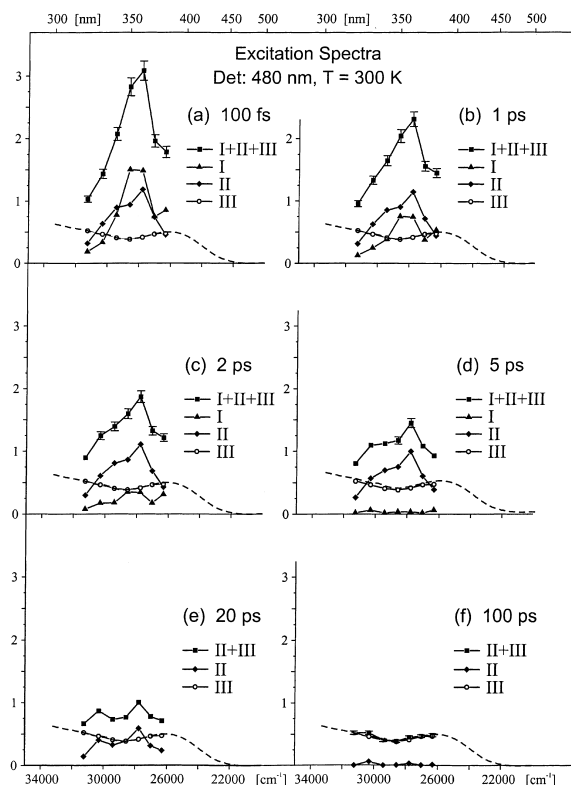
Fig. 5. Reconstructed excitation spectra of a 150 nm thin Alq$_3$ film on a quartz substrate following time-resolved detection of fluorescence. Time range from 100 fs to 100 ps, detected at 480 nm, $T = 300$ K. The times for the delayed detection are indicated in the panels. The squares represent the data points obtained after spectral reconstruction for the total intensity of the excitation spectrum, $I(\lambda, t) = a_1(\lambda) \exp(-t/\tau_1) + a_2(\lambda) \exp(-t/\tau_2) + a_3(\lambda) \exp(-t/\tau_3)$. The triangles represent the reconstructed point-to-point excitation spectrum (band I) resulting for the single exponential decay with τ_1, the diamonds represent the reconstructed point-to-point excitation spectrum (band II) resulting for the single exponential decay with τ_2, the open circles represent the reconstructed point-to-point excitation spectrum (band III) resulting for a single exponential decay with τ_3. The dashed curve is the cw-absorption spectrum.

Alq$_3$-film on quartz
Exc: 350 nm, Det: 493 nm

τ_1 = 0.9 ps (46 %)
τ_2 = 15.0 ps (32 %)
τ_3 = 10.0 ns (22 %)

(a) T = 300 K

τ_1 = 2.9 ps (21 %)
τ_2 = 58.2 ps (34 %)
τ_3 = 13.5 ns (22 %)

(b) T = 105 K

τ_1 = 2.2 ps (20 %)
τ_2 = 109.0 ps (36 %)
τ_3 = 14.0 ns (44 %)

(c) T = 75 K

τ_2 = 34.0 ps (20 %)
τ_3 = 16.5 ns (80 %)

(d) T = 4.2 K
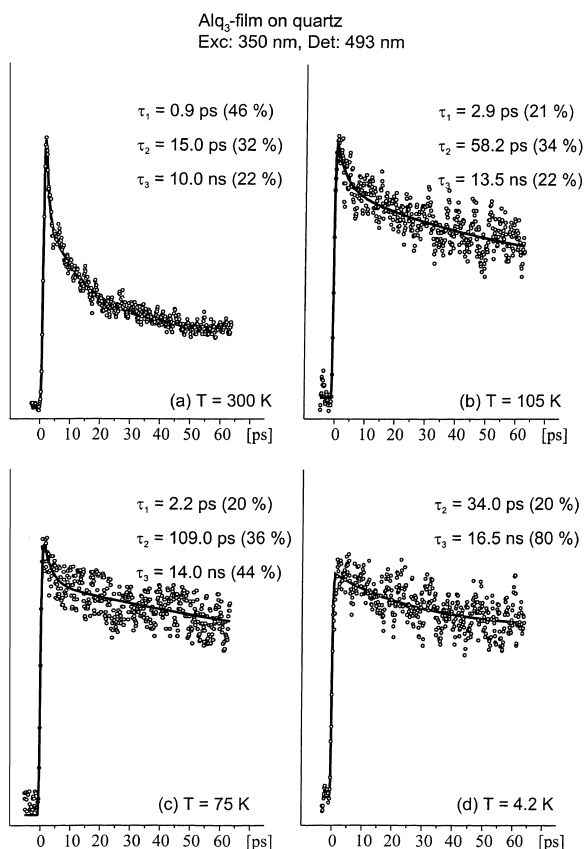
Fig. 6. Representative fluorescence transients of a 150 nm thin Alq$_3$ film on a quartz substrate for different temperatures, excitation at 350 nm, detection at 493 nm. Drawn curves represent best fits as described in the text. Respective time constants and pre-exponential factors are also given in Table 3.

Representative transients are shown in Fig. 6. The respective time components and pre-exponential factors are summarized in Table 3.

4. Discussion

For Alq$_3$, it has been discussed that the fluorescent state is a $^1\pi\pi^*$ state localized at one of the quinolinolate ligands and that intraligand electronic charge transfer has taken place from the phenoxide to the pyridyl rings of the ligand [2,5,14–17].

From the fits of the time-resolved data, presented in Section 3, it is found that the initial emission of vapor-deposited Alq$_3$ films, consists of a superposition of three independent emission bands (cf. Fig. 3a). We label the emission bands as band I (maximum at 21 130 cm^{-1}), band II (maximum at 20 640 cm^{-1}) and band III (maximum at 18 850 cm^{-1}). The sum of all three log-normal line shapes fits the reconstructed point-to-point spectrum of the total emission. Up to 2 ps, all reconstructed spectra are a superposition of the aforementioned three bands I–III (Fig. 3a–c). Band I decays with a characteristic time of about 1 ps; thus, after about 5 ps, the reconstructed spectrum is only a superposition of bands II and III (Fig. 3d). At 100 ps, after the excitation pulse, the reconstructed spectrum can be fitted to a single log-normal line shape function, the same as for band III (Fig. 3f), because bands I and II no longer contribute. Emission band III, with its maximum at 18 850 cm^{-1}, coincides with the cw-emission spectrum of an Alq$_3$ film at room temperature (cf. Figs. 1 and 3f). Thus, the cw-emission consists mainly of the band III emission. It is remarked that the result that the transient emission consists of three components is independent of the exact choice for the emission band line shape functions, i.e., even if it is preferred to simulate the emission with line shape functions other than log-normal functions.

As already noted, the reconstructed spectra of Fig. 3 fit log-normal line shape functions. It is well known [21] that log-normal shape functions are characterized by parameters that determine the peak position, the band width and the band asymmetry. Within the context of this paper, however, it suffices to note that the experimental fluorescence transients give rise to three emission bands (I–III) and that each of these bands shows its own kinetics. A further analysis of the log-normal parameters is outside the scope of this paper.

We now compare the reconstructed excitation spectra after delayed detection of the emission (Fig. 5) to the cw-absorption spectrum of an Alq$_3$ film on a quartz substrate. It is seen that the reconstructed excitation spectrum for emission bands I and II at early delay times (<5 ps) gives rise to a new absorption, not observed in the cw absorption, with a maximum near 350 nm

Table 3
Time components (τ_i) and pre-exponential factors (a_i) for different temperatures obtained from the fit of fluorescence decays of Alq$_3$ films on a quartz substrate measured by upconversion technique in a time window of 60 ps at different temperatures (system response time: 150 fs, $\lambda_{det} = 493$ nm, $\lambda_{exc} = 350$ nm)[a]

Temperature (K)	τ_1 (ps) (a_1)	τ_2 (ps) (a_2)	τ_3 (ns) (a_3)	τ_{av} (ps)
300	0.9 (46%)	15.0 (32%)	10.0 (22%)	6.7
248	1.2 (42%)	19.0 (35%)	11.0 (23%)	9.3
223	1.4 (40%)	24.0 (38%)	12.0 (22%)	12.4
198	1.3 (42%)	24.0 (31%)	12.5 (26%)	10.9
173	1.3 (39%)	27.9 (34%)	13.0 (27%)	13.7
148	1.1 (36%)	31.5 (33%)	13.5 (31%)	15.6
105	2.9 (21%)	58.2 (34%)	13.5 (45%)	37.1
75	2.2 (20%)	109.0 (36%)	14.0 (44%)	70.8
4.2	–	34.0 (20%)	16.5 (80%)	–

[a] Additionally, the weighted average lifetime $\tau_{av} = (a_1\tau_1 + a_2\tau_2)/(a_1 + a_2)$ is included.

($\approx 28\,500$ cm^{-1}). In the investigated time window from 100 fs to 100 ps (cf. Fig. 5a–f), the excitation spectrum of band III matches the shape of the cw-absorption spectrum. We conclude from the laser-pulse experiments that there are two short-lived emissive shallow-trap species, I and II, exhibiting independent absorption and emission bands, with maxima shifted to higher energies (by about 2000 cm^{-1}) compared to the emission and absorption band positions of the emissive deep-trap species, labeled III.

The observation of several emission decay components at early times may not be surprising considering that the Alq$_3$ film is amorphous. Trapping sites with non-uniform structures in Alq$_3$ films have been reported by Burrows et al. [4]. As common for low-mobility organic solids, the emission from the vapor deposited thin films was contributed to small-radius Frenkel excitons [22] trapped in the neighborhood of imperfections in the film. Another factor of importance for the occurrence of different emissive species may be the molecular structure of the Alq$_3$ tris-chelate complex. The two geometrical isomers of Alq$_3$, the "meridianal" (mer) and the "facial" (fac) isomer, are chiral and thus correspond to two different optical isomers. DFT-based calculations [15] predict that the mer isomer is lower in energy, but fac has a higher dipole moment, and it is reasonable to expect that in the condensed phase both isomers may coexist. The disorder of the Alq$_3$ molecular structure in the film may also be the cause for the presence of different trapping sites. As has been reviewed recently [23], in an amorphous molecular solid (with a high density of sites), static disorder influences the diagonal and non-diagonal elements of the energy matrix as well as the density-of-states (DOS) of the resulting inhomogeneous spread of optically active sites. The excited-state dynamics of the multi-molecular system then sensitively depends on the excitation energy: when excitation is above a certain (threshold) energy of the many-particle system, intersite transport will give rise to relaxation to lower Frenkel-type localized (quasi-exciton) states so that eventually the excitation becomes trapped. If, on the other hand, excitation is below the threshold energy, transfer to low-energy tail states during the lifetime of the excited states is hampered (due to the low DOS value) and the excitation remains at the localized (molecular or quasi-excitonic) state. We attribute the occurrence of bands I and II to the existence of trapped (quasi-) excitons (with emission band maxima at 21 130 and 20 640 cm^{-1}), whereas band III (at 18 850 cm^{-1}) is from a relatively deep trap below the quasi-exciton band. Obviously, in the amorphous film, a large variety of different trapping sites may be present, giving rise to a spread in emissive lifetimes. Thus, the emission decay may not exist just for three components, as discussed above, but may be composed of many more components. Effectively, however, it is justified to say that the Alq$_3$ films contain short-lived emissive centers with typical lifetimes, at room temperature, of the order of 1–20 ps and deep traps with typical lifetimes of about 10 ns.

It is remarked in passing that one may wonder if the data and their analysis obtained with the femtosecond upconversion technique could be independently verified, for instance, by transient absorption measurements. Results from transient absorption measurements are expected to be hard to analyze because of complications caused by bleaching of ground state absorption, and superposition of different excited state absorptions of the different traps. On the other hand, the fluorescence upconversion technique has the advantage that one can exclusively probe the time dependence of the excited-state population without interference of the aforementioned bleaching and excited-state absorptions.

The much shorter lifetimes of bands I and II (in the picosecond regime) in comparison to the lifetime of band III ($\sim$10 ns) are indicative of an additional non-radiative decay channel for the shallow traps. The weighted average lifetime of the shallow trap emission, i.e., $\tau_{av} = (a_1\tau_1 + a_2\tau_2)/(a_1 + a_2)$, is temperature dependent (Table 3 and Fig. 6). This is suggestive of an additional thermally activated relaxation for the shallow trap species. The shallow traps might be depleted by thermal excitation into what we loosely call the (quasi-) exciton band. Since excitons are far more delocalized than the trap excitations, the thermally excited excitons could be almost instantaneously re-trapped at non-emissive other sites. This would explain that the exciton emission itself remains absent and also that the shallow trap emission becomes thermally quenched.

In a simplified approach, we now consider the decay of the shallow traps to be represented by just one effective decay rate constant k_S^{tot} (equal to τ_{av}^{-1}). The effective decay rate constant is given as

$$k_S^{tot} = k_S + k_T \exp\left(-\Delta E_{act}/k_B T\right), \qquad (2)$$

where k_S is the effective decay rate constant of the shallow traps in the absence of thermal detrapping, k_T is the rate constant for detrapping to the exciton band, and ΔE_{act} is the average energy gap between the shallow traps and the lower edge of the exciton band. From an Arrhenius plot of k_S^{tot} as a function of temperature (cf. Fig. 7, the experimental values of k_S^{tot} were obtained from the values
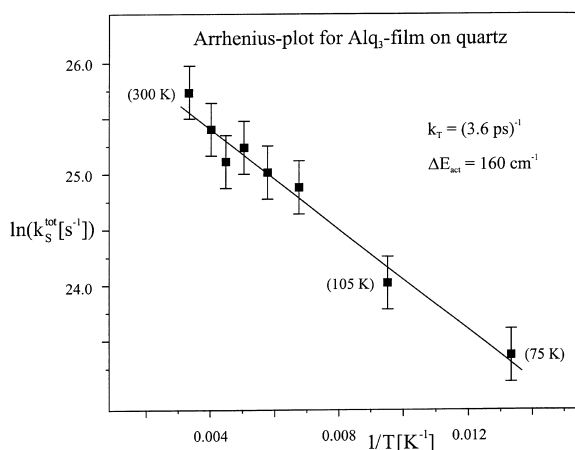
Fig. 7. Arrhenius plot for the weighted average decay rate of the shallow trap emission of a 150 nm thin Alq$_3$ film on a quartz substrate versus the temperature, following Eq. (2). The resulting parameters for the linear fit (—) are given in the text (Section 4).

of τ_{av} in Table 3), we find, $k_T = (3.6\ \text{ps})^{-1}$ and $\Delta E_{act} = 160\ \text{cm}^{-1}$, while k_S is proposed to be in the order of the deep trap deactivation rate $\sim$(10 ns)$^{-1}$.

Finally, we consider the disparity in lifetimes for the shallow and deep traps. Assuming thermal equilibrium, one has $\Delta E = k_B T \ln\left(k_S^{tot}/k_D\right)$, where ΔE is the energy separation between the shallow and deep traps, k_D is the inverse decay time of the deep trap. At 300 K, we have $k_S^{tot} = 1\ \text{ps}^{-1}$ and $k_D = 0.1\ \text{ns}^{-1}$, and we find $\Delta E = 1920\ \text{cm}^{-1}$. This value is in good agreement with the energy separation of 2000 cm^{-1} between the average position of bands I and II on the one hand and the position of band III on the other hand (cf. Fig. 3). The scheme in Fig. 8 summarizes our main results.

In summary, femto- and pico-second time-resolved fluorescence experiments show that the emissive behavior of vapor-deposited thin Alq$_3$ films, to a large extent, is determined by trapping sites. The fluorescence of Alq$_3$ films exhibits a multi-exponential (sub)picosecond decay typical of a distribution of emissive shallow and deep trapping sites differing in energy by about 2000 cm^{-1}. At temperatures above 75 K, the efficiency of the photoluminescence is reduced by thermal depletion of the shallow traps into non-radiative decay channels.

Energy level scheme for Alq₃-film on quartz
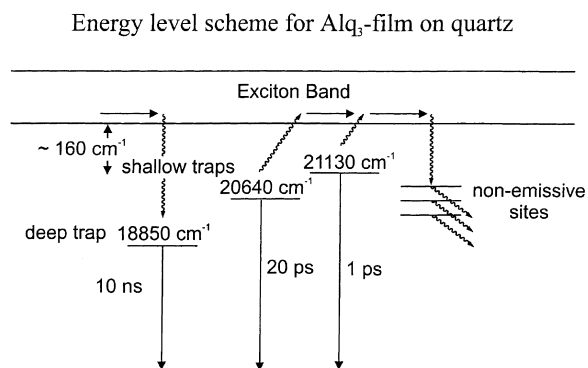
Fig. 8. Energy level scheme for the trap distribution and the dynamical processes (at room temperature) for a 150 nm thin Alq₃ film on a quartz substrate.

References

[1] C.W. Tang, S.A. van Slyke, C.H. Chen, J. Appl. Phys. 65 (1989) 3610.
[2] P.E. Burrows, L.S. Sapochak, D.M. McCarty, S.R. Forrest, M.E. Thompson, Appl. Phys. Lett. 64 (1994) 2718.
[3] J. Kido, M. Kimura, K. Nagai, Science 267 (1995) 1332.
[4] P.E. Burrows, Z. Shen, V. Bulovic, D.M. McCarty, S.R. Forrest, J.A. Cronin, M.E. Thompson, J. Appl. Phys. 79 (1996) 7991.
[5] J.R. Sheats, H. Antoniadis, M. Hueschen, W. Leonard, J. Miller, R. Moon, D. Roitman, A. Stocking, Science 273 (1996) 884.
[6] S.E. Shaheen, G.E. Jabbour, B. Kippelen, N. Peyghambarian, J.D. Anderson, S.R. Marder, N.R. Armstrong, E. Bellmann, R.H. Grubbs, Appl. Phys. Lett. 74 (1999) 3212.
[7] H. Mattoussi, H. Murata, C.D. Merritt, Y. Iizumi, J. Kido, Z.H. Kafafi, J. Appl. Phys. 86 (1999) 2642.
[8] H. Sixl, H. Schenk, N. Yu, Phys. Bl. 54 (3) (1998) 225.
[9] R. Ballardini, G. Varani, M.T. Indelli, F. Scandola, Inorg. Chem. 25 (1986) 3858.
[10] A.D. Walser, I. Sokolik, R. Priestley, R. Dorsinville, Synthetic Metals 84 (1997) 877.
[11] R. Priestley, I. Sokolik, A.D. Walser, C.W. Tang, R. Dorsinville, Synthetic Metals 84 (1997) 915.
[12] R. Priestley, A.D. Walser, R. Dorsinville, Optics Commun. 158 (1998) 93.
[13] L.-J. Lin, S.A. Jenekhe, R.H. Young, P.M. Borsenberger, Appl. Phys. Lett. 70 (1997) 2052.
[14] W. Stampor, J. Kalinowski, G. Marconi, P. Di Marco, V. Fattori, G. Giro, Chem. Phys. Lett. 283 (1998) 373.
[15] A. Curioni, M. Boero, W. Andreoni, Chem. Phys. Lett. 294 (1998) 263.
[16] F.E. Lytle, D.R. Storey, M.E. Juricich, Spectrochim. Acta 29A (1973) 1357.
[17] W. Humbs, E. van Veldhoven, H. Zhang, M. Glasbeek, Chem. Phys. Lett. 304 (1999) 10.
[18] E.R. Middelhoek, P. van der Meulen, J.W. Verhoeven, M. Glasbeek, Chem. Phys. 198 (1995) 573.
[19] M.A. Kahlow, W. Jarzeba, T.P. Dubrull, P.F. Barbara, Rev. Sci. Instrum. 59 (1988) 1098.
[20] H. Zhang, A.M. Jonkman, P. van der Meulen, M. Glasbeek, Chem. Phys. Lett. 224 (1994) 551.
[21] M. Maroncelli, G.R. Fleming, J. Chem. Phys. 86 (1987) 6221.
[22] M. Pope, C.E. Swenberg, Electronic Processes in Organic Crystals, Clarendon Press, Oxford, 1982.
[23] H. Bässler, B. Schweitzer, Acc. Chem. Res. 32 (1999) 173.